

A simplified model for the assessment of the impact probability of fragments

Gianfilippo Gubinelli^a, Severino Zanelli^a, Valerio Cozzani^{b,*}

^a *Dipartimento di Ingegneria Chimica, Chimica Industriale e Scienza dei Materiali, Università degli Studi di Pisa, via Diotisalvi n.2, 56126 Pisa, Italy*

^b *Dipartimento di Ingegneria Chimica, Mineraria e delle Tecnologie Ambientali, Università degli Studi di Bologna, viale Risorgimento n.2, 40136 Bologna, Italy*

Received 8 May 2004; received in revised form 29 August 2004; accepted 4 September 2004

Available online 19 October 2004

Abstract

A model was developed for the assessment of fragment impact probability on a target vessel, following the collapse and fragmentation of a primary vessel due to internal pressure. The model provides the probability of impact of a fragment with defined shape, mass and initial velocity on a target of a known shape and at a given position with respect to the source point. The model is based on the ballistic analysis of the fragment trajectory and on the determination of impact probabilities by the analysis of initial direction of fragment flight. The model was validated using available literature data.

© 2004 Elsevier B.V. All rights reserved.

Keywords: Domino effect; Fragments; Missiles; Explosion; Consequence assessment

1. Introduction

The generation of missiles usually follows the catastrophic rupture of process equipment due to internal pressure exceeding design values. Among the several possible causes of vessel fragmentation, two accidental scenarios are responsible of most of the primary accidents resulting in fragment projection: internal explosions due to confined deflagrations and BLEVEs.

The projection of fragments is one of the more important causes of domino effects in industrial accidents [1–6]. Fragments are capable of generating secondary accidents at relevant distances from the primary scenario. Thus, safety distance criteria and preventive actions to avoid domino effect can hardly be applied [6]. In this framework, quantitative risk analysis (QRA) may provide useful criteria for the assessment of domino scenarios caused by fragment projection, based on both expected frequency and expected conse-

quence assessment [7–9]. Nevertheless, the estimation of the expected frequencies of domino scenarios caused by equipment fragmentation requires the availability of a model for the assessment of fragments impact probabilities on a given target.

Several sources report data on missile projection due to vessel fragmentation [1,10–12]. In particular, a comprehensive analysis of pressurised liquefied gas vessels fragmentation may be found in the study of Holden and Reeves [11] that proposed models for the probability of fragment projection, the estimation of the number of fragments generated and the distribution of fragment projection distances. A few models were proposed for fragment impact probability or for maximum fragment flight distance based on a direct statistic analysis of post-accident data [10,12]. However, these were developed from the analysis of a limited number of case histories, mainly concerning LPG vessels. Their possible extension to the study of a generic vessel fragmentation without a previous validation still needs to be verified.

As underlined by Lees [1], the flight of a fragment is a standard problem in mechanics for which a fundamental approach

* Corresponding author. Tel.: +39 051 2093141; fax: +39 051 581200.
E-mail address: valerio.cozzani@mail.ing.unibo.it (V. Cozzani).

Nomenclature

| | |
|----------------------|--|
| A_D | Fragment projection area on a plane perpendicular to the trajectory (m^2) |
| C_D | A dimensional drag coefficient |
| d | Initial direction of projection of the fragment |
| D | Distance of the target axis from the explosion center (m) |
| D_e | Fragment external diameter (m) |
| DF | Drag factor used in [13] |
| D_{max} | Maximum distance achievable by the fragment (m) |
| D_{min} | Target minimum distance from the explosion center (m) |
| F | Fraction of fragments projected at distances lower than a defined distance R |
| f_d | Domino effect frequency (events/year) |
| $f_{d,F}$ | Frequency of the domino effect due to a specific fragment (events/year) |
| f_p | Primary event frequency (events/year) |
| g | Gravitational acceleration (m/s^2) |
| H_T | Target height (m) |
| k | Drag factor used in the present article (m^{-1}) |
| M | Fragment mass (kg) |
| $P_{d,F}$ | Domino effect probability due to a specific fragment |
| $P_{dam,F}$ | Damage probability of a target due to a specific fragment impact |
| φ_{dir} | Probability distribution for the initial direction of fragment projection |
| $P_{F,d}$ | Probability of projection of the fragment in a direction d |
| $P_{gen,F}$ | Probability of generation of a specific fragment |
| $P_{imp,F}$ | Impact probability of a specific fragment on the target |
| R_T | Target radius (m) |
| t | Fragment thickness (m) |
| u | Initial velocity of the fragment (m/s) |
| u_{max} | Maximum initial velocity of the fragment (m/s) |
| V | Vessel volume (m^3) |
| <i>Greek symbols</i> | |
| φ | Angle used to define the initial direction of fragment projection d |
| θ | Angle used to define the initial direction of fragment projection d |

is described by Baker et al. [13]. However, the method proposed by these authors is concerned with the accurate determination of the trajectory of a fragment, and it is not suitable to derive the impact probability of a fragment. Hauptmanns [14,15] proposed a valuable and comprehensive approach to the calculation of impact probabilities of a fragment based

on trajectory analysis. Impact probabilities in a given position with respect to the fragment origin were calculated by Monte Carlo methods, assuming probability distributions for the initial projection parameters (e.g. initial fragment velocity, number, mass and energy of fragments, etc.). Nevertheless, the study was mainly oriented to the determination of impact probabilities on exposed individuals and not on process equipment, thus the influence of the target geometry was not taken into account.

Therefore, a general method for the assessment of the probability of domino scenarios caused by fragment impact is not yet available. This study specifically addresses one of the necessary steps within the development of a comprehensive model for domino probabilities due to fragment projection: the evaluation of the impact probability of a fragment on a given target. The study was based on a ballistic analysis of all the possible trajectories of a fragment with a given mass, shape and initial velocity. A simplified analytic function was obtained for the trajectory and was validated using the results of the detailed model given by Baker et al. [13]. This made possible a probabilistic approach to the estimation of the projection distance and direction. The impact condition was verified taking into account the actual target geometry and its distance from the fragment source. A sensitivity analysis was performed, in order to identify the relevant model parameters and the accuracy needed for the different input values. A comparison with data from past accidents [11] allowed the preliminary validation of the model.

2. Probability of domino effect due to fragments

The frequency of a domino event caused by the impact of a fragment generated in a primary accident on a given secondary target may be expressed as:

$$f_d = f_p \times P_d \quad (1)$$

where f_p is the expected frequency of the primary event, and P_d expresses the probability of the following event sequence, necessary to cause a domino effect, given the primary accident:

1. generation of several fragments of defined mass and shape during the primary event;
2. projection of the fragments with an initial velocity different for each fragment;
3. impact of one (or more than one) of the fragments with the given target;
4. loss of containment of the target caused by the fragment impact.

Each fragment generated in the primary event may cause a domino effect with an expected frequency given by the following expression:

$$f_{d,F} = f_p \times P_{d,F} \quad (2)$$

where $P_{d,F}$ is the probability of the above event sequence for a single fragment. This may be expressed as:

$$P_{d,F} = P_{gen,F} \times P_{imp,F} \times P_{dam,F} \tag{3}$$

where

- $P_{gen,F}$ is the probability of the fragment F (with defined mass, shape and initial velocity) to be generated in the primary event;
- $P_{imp,F}$ is the probability of impact between the fragment and a target;
- $P_{dam,F}$ is the probability of target damage given the impact with the fragment.

If the probability that two fragments impact on the same target is sufficiently low, as usual if a limited number of fragments is generated in the primary event, the expected frequency of a domino event caused by fragments impacting on a given secondary target, f_d , could be calculated as follows:

$$f_d = \sum_F f_{d,F} = f_p \sum_F P_{d,F} \tag{4}$$

and using Eq. (1), the probability P_d becomes:

$$P_d = \sum_F P_{d,F} \tag{5}$$

The above approach shows that the probability of a domino effect due to the generation of fragments in the primary event may be estimated if it is possible to evaluate the number of fragments that are likely to be generated in the primary event, and the probabilities $P_{gen,F}$, $P_{imp,F}$, and $P_{dam,F}$ for each of the fragment projected in the primary event.

The present study focused on the estimation of the impact probability ($P_{imp,F}$) of a fragment with defined shape, mass and initial velocity on a given target. The development of a model for the quantitative estimation of $P_{imp,F}$ is an important step needed towards the development of a comprehensive model for the quantitative assessment of risk due to domino accidents caused by missiles projection.

The determination of the other two conditional probabilities needed in order to calculate the overall domino probability, $P_{gen,F}$ and $P_{dam,F}$, falls out of the scope of the present study. However, in the literature several approaches were proposed to estimate these parameters. In particular, the methods of Scilly and Crowter [12] and of Holden and Reeves [11] provide an approach based on the statistical analysis of past accidents in order to estimate the number and the weight of the fragments generated in the fragmentation of vessels. On the other hand, scarce attention was devoted to the determination of damage probability following the impact of a fragment. Several models are available for the calculation of fragment penetration on a given target [1,13], but no criteria are provided for the estimation of damage probability. A usual conservative hypothesis is to assume a unit value for this probability [1].

3. Modelling fragment impact probability

3.1. Reference system and simplifying assumptions

It is well known that the behaviour of a projected fragment is influenced by its shape and its instantaneous velocity, due to the complex interaction of gravitational and fluidodynamic forces [1,13]. The trajectory and velocity of the mass centre of the fragment were used in the following to describe the trajectory and velocity of the entire fragment.

Fig. 1(a) schematises a possible impact condition of a fragment F with defined mass, shape and initial velocity \mathbf{u} on a target. The point O, that is the initial position of the centre of mass of the generated missile (coincident with the position of the process vessel that undergoes the primary accident) was assumed as the origin of the absolute reference system $x'y'z'$, where $x'z'$ is a plane parallel to the ground and the y' -axis has an opposite direction with respect to the gravitational acceleration vector \mathbf{g} . In this reference system, a vector \mathbf{d} of unitary modulus was defined, representing the initial direction of the fragment. The vector \mathbf{d} has the following components with respect to directional angles θ and φ (see Fig. 1(a)):

$$\mathbf{d} = \begin{bmatrix} \cos(\theta) \cos(\varphi) \\ \sin(\varphi) \\ \sin(\theta) \cos(\varphi) \end{bmatrix}$$

The initial velocity \mathbf{u} could thus be expressed as $\mathbf{u} = u\mathbf{d}$.

A second reference system, xyz , was also defined, in which the trajectory of the centre of mass belongs to the xy plane. This corresponds to a rotation of the absolute reference

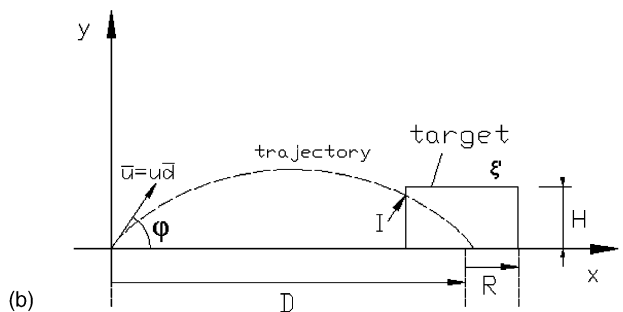
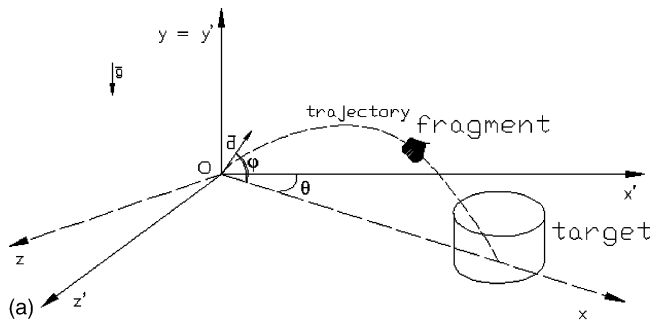


Fig. 1. Schematisation adopted to represent the trajectory of a fragment and of the impact on a given target. (a) Reference coordinate systems; (b) representation of the trajectory on the xy plane.

system of an angle θ around the y' -axis. This second reference system has the same origin of the $x'y'z'$ system, and the y -axis has the same direction of y' . Obviously, this schematisation requires to neglect the deviations of the centre of mass due to the wind and to the possible oscillations caused by rotational movements of the fragment. However, the velocity of the missiles is usually higher of more than an order of magnitude than normal wind velocities. Moreover, the rotational movements of the fragment are likely to cause an oscillation of the mass centre around its main direction. Thus, with a reasonable approximation, the fragment trajectory could be represented on a single xy plane, as shown in Fig. 1(b).

Some assumptions were also introduced in order to simplify the impact condition of the fragment on a given target. As a matter of fact, in the calculation of impact probability on human targets, e.g. within the calculation of individual risk, the size of the target may be neglected and the impact probability is calculated as the probability of the fragment centre of mass to return on the ground in a generic (x, z) position. On the other hand, if the probability of impact with an equipment item as a storage vessel or a column is of interest, the geometry of the target should be taken into account. In particular, in the case of equipment having a relevant elevation above ground level, as columns, the shape of the target highly influences the impact probability.

Thus, as shown in the schematisation given in Fig. 1(b), in the present approach the impact was considered to take place if an intersection point I exists between the trajectory of the mass centre and the target profile on the xy plane. The target profile on the xy plane, however, is in general a function of the angle θ . In the present approach, the dependence on the angle θ was eliminated, considering for any θ value a constant rectangular profile (see Fig. 1(b)), defined by the maximum height of the target, H , and the maximum width in the radial direction (equal to the diameter of the profile if a cylindrical tank with a vertical axis is considered). This conservative approximation is partially compensated neglecting the actual shape of the fragment in the impact condition. As stated above, only the trajectory of the fragment mass centre was considered in order to verify the impact condition. This further simplification may be justified considering that usually fragments are quite smaller than the targets of concern considered in the present analysis (process equipment or storage tanks with a relevant inventory). It must be remarked, however, that the actual size and shape of the fragment were neglected only in order to verify the impact condition.

3.2. Impact probability

On the basis of the above assumptions, the impact probability of a fragment F (with defined mass, shape and initial velocity) on a given target is thus dependent only on the probability of the initial direction \mathbf{d} . The probability that the fragment will be projected with an initial direction \mathbf{d} may be thus expressed as a function of the directional angles θ

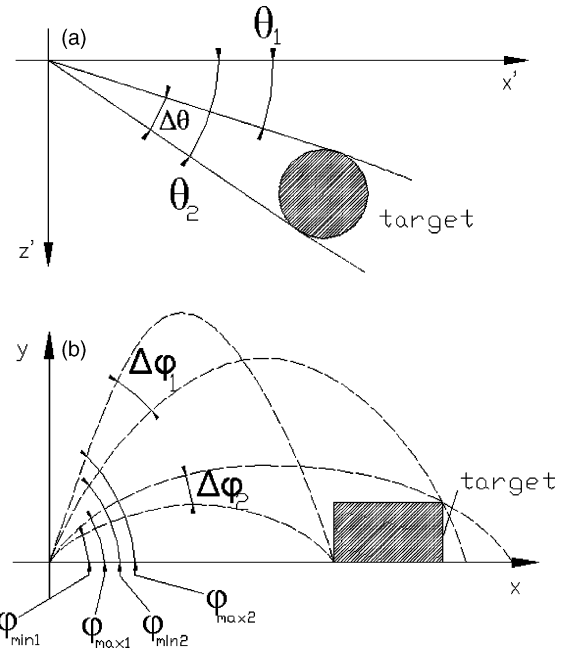


Fig. 2. Angles of impact on the $x'z'$ plane (a) and on the xy plane (b).

and φ :

$$P_{F,d}(\theta, \varphi) = \wp(\theta, \varphi) \times d\theta \times d\varphi \quad (6)$$

where $\wp(\theta, \varphi)$ is the probability distribution of the fragment initial direction. Defining $\Delta\theta$ and $\Delta\varphi$ as the intervals identifying all the directional angles θ and φ for which the impact takes place, as shown in Fig. 2, the total impact probability of the fragment F on the target may be expressed as follows:

$$P_{imp,F} = \int_{\Delta\theta} \int_{\Delta\varphi} \wp_{dir}(\theta, \varphi) \times d\theta \times d\varphi \quad (7)$$

3.3. Probability distribution of the initial missile direction

The direction of fragment projection may depend on several factors, as the features of the ruptured vessel, the position of the main pipes, the characteristics of the explosion causing the generation of the fragments, etc. Although the study of a specific layout may yield more precise information on the possible directions available for fragment projection, this approach is not feasible in a QRA framework of a complex plant. Thus, unless precise information is available on the presence of preferential directions for fragments projection, a uniform probability distribution may be assumed. In the previous paragraph it was shown that the initial direction \mathbf{d} may be described using the angles φ and θ , with φ values ranging between $-\pi/2$ and $\pi/2$, and θ values between 0 and 2π . Also, the probability distribution may be expressed as a function of φ and θ . As a matter of fact, if a spherical surface of radius r is considered and a uniform probability distribution is assumed, the probability of the fragment to be projected with

initial direction \mathbf{d} equals the ratio between an infinitesimal surface dA identifying the initial direction of interest and the total surface of a sphere of radius r :

$$\wp(\theta, \varphi) \times d\theta \times d\varphi = \frac{dA}{4\pi r^2} = \frac{\cos \varphi d\varphi d\theta}{4\pi} \quad (8)$$

Thus, Eq. (7) may be rewritten as follows:

$$P_{\text{imp,F}} = \frac{1}{4\pi} \int_{\Delta\theta} \int_{\Delta\varphi} d\theta \times \cos(\varphi) d\varphi \quad (9)$$

However, the φ intervals that verify the impact condition are not dependent on θ if the simplified impact condition discussed in Section 3.1 is introduced. Thus, Eq. (9) may be simplified as follows:

$$P_{\text{imp,F}} = \frac{\Delta\theta}{4\pi} \int_{\Delta\varphi} \cos(\varphi) d\varphi \quad (10)$$

Obviously, the intervals $\Delta\theta$ and $\Delta\varphi$ should be calculated on the basis of the impact condition and of the fragment trajectory.

3.4. Fragment initial velocity

The initial velocity of the fragment, required to use the model developed in the present approach, should be estimated using specific methods. Several models are proposed in the literature for the evaluation of the initial velocity of fragments [13,16–20]. Table 1 summarizes the models more frequently used and the available criteria for model selection, while a comprehensive review of these methods can be found elsewhere [10,21].

3.5. Fragment trajectory

The availability of a model for fragment trajectory is the more delicate step in order to assess the probability of a fragment to impact on a given target. Several models were pro-

posed in the literature for the description of the trajectory of projected fragments. A comprehensive review is given by Lees [1]. Baker et al. [13] developed a fundamental approach to the problem, based on the description of the fragment motion considering the fragment acceleration and three type of forces acting on the fragment: gravitational, drag and lift forces. The last two were expressed as a function of the shape, the mass and the orientation of the fragment with respect to the trajectory of its mass centre. The trajectory of the fragment was represented by that of its mass centre. However, the model of Baker et al. [13] has two important drawbacks in the framework of the present study:

- the model needs two uncertain input parameters: the shape of the fragment and its orientation with respect to the velocity vector;
- the model may be used only solving by numerical methods the differential balance equations on which it is based.

In a QRA framework, it is necessary to limit the detail of the inputs required in order to limit the time requirements and the complexity of the analysis. Moreover, since a probabilistic approach to the problem is of concern in the present study, the availability of an analytical function for fragment trajectory would contribute to simplify the problem. Thus, following also the approach proposed by Hauptmanns [14], the description of the trajectory was based on the more simple equations generally used in mechanics to describe the motion of objects with velocities in the subsonic range:

$$\frac{d^2x}{dt^2} + k \left(\frac{dx}{dt} \right)^2 = 0 \quad (11)$$

$$\frac{d^2y}{dt^2} + (-1)^n k \left(\frac{dy}{dt} \right)^2 + g = 0 \quad (12)$$

where x and y are the coordinates of the position of the fragment at time t , g is the gravitational acceleration, k is a drag factor, and n equals 1 in the descending part of the trajectory and 2 in the ascending part. As previously stated, the above

Table 1
Available methods to evaluate the initial velocity of fragments

| | Model equations | References | Suggested applications |
|---|--|------------|---|
| 1 | $u = (2E_K/M)^{0.5}$; $E_K = \alpha E$ | [13,16,17] | $E_s < 0.8$, all vessels [10,21] |
| 2 | Graphical method. Upper limits derived from Baker et al. [13]: $\log(u_s) = 0.56 \log(P_s) + 0.23$ cylind. vessels $\log(u_s) = 0.6 \log(P_s) + 0.13$ spheric. vessels $P_s = (P_1 - P_0)V/(M_V a_0^2)$ $u_s = u/(ka_0)$ | [13,18] | $E_s < 0.8$, pressurised vessel burst, runaway reaction, internal explosion, gas filled vessel [10,13,18,21] |
| 3 | $u = 0.88a_0 F^{0.55}$ $F = (P_1 - P_0)AR/(Ma_0^2)$ | [19] | $E_s < 0.8$, cylindrical and spherical vessel (ideal gas) [10]. |
| 4 | $u = 1.092(EG/M_V)$ $G = 1/(1 + C/2M_V)$ cylindrical vessels $G = 1/(1 + 3C/5M_V)$ spherical vessels | [20] | $E_s > 0.8$, high energy explosion [10] |

E : explosion energy; E_K : kinetic energy; M_V : vessel mass; P_1 : pressure inside vessel at failure; P_0 : atmospheric pressure; a_0 : sound velocity in the gas; A : area of detached portion of vessel wall; R : radius of vessel; M : fragment mass; C : total mass of gas; E_s : scaled explosion energy, $E_s = 2E/(M_V a_0^2)$.

equations are only valid for subsonic velocities of the fragment. However, this limitation seems not important, since the initial fragment velocities are estimated to be usually lower than 200 m/s [10,21–24].

The terms multiplying k identify the drag forces exerted on the object in the x and y directions. In the subsonic range, these forces should be proportional, by a factor k independent of the direction, to the square of the instantaneous velocity of the object. The factor k is a function of the mass and the shape of the fragment.

The main problem in the use of the above model is in the determination of the drag constant k , that is the only model parameter and that heavily influences the model results. In the present approach, k was used as a fitting parameter. A simple technique was developed in order to estimate the value of k that, for all the possible initial fragment velocities, yields a maximum fragment fly distance equivalent to that predicted by the model of Baker et al. [13]. This was possible since the analysis of past accidents showed that most of the fragments generated in the explosion of process vessels are usually ‘chunky’ in shape [13]. For chunky fragments, in the model of Baker et al. [13] the following drag factor is defined:

$$DF = \frac{C_D A_D}{M} \quad (13)$$

where C_D is a drag coefficient, function of the fragment shape and of its orientation with respect to the flow condition, A_D the section of the fragment on a plane perpendicular to the trajectory and M is the mass of the fragments. The equivalent drag factor k that in the present approach yields the same maximum distances if used in Eqs. (11) and (12) may be calculated by the following expression:

$$k = a \times DF - b \quad (14)$$

where a and b are dimensional constants ($a = 0.69 \text{ kg/m}^3$ and $b = 3.28 \times 10^{-5} \text{ m}^{-1}$). Since the orientation of the fragment with respect to the trajectory is usually unknown, an average value of DF may be used in Eq. (14):

$$DF_a = \frac{DF_{\max} + DF_{\min}}{2} \quad (15)$$

where DF_{\min} and DF_{\max} are respectively the minimum and the maximum values of DF that may be obtained considering all the possible orientations of the fragment. Once the drag factor k is determined and a value for the initial velocity u of the fragment is assumed, an analytical expression of the trajectory may be easily obtained solving Eqs. (11) and (12). The analytical expression of fragment trajectory is reported in appendix A. This function was used to calculate the $\Delta\theta$ and $\Delta\varphi$ intervals that verify the impact condition discussed in Section 3.1. A specific software program was developed, yielding the $\Delta\theta$ and $\Delta\varphi$ intervals as a function of k and u (see Fig. 2).

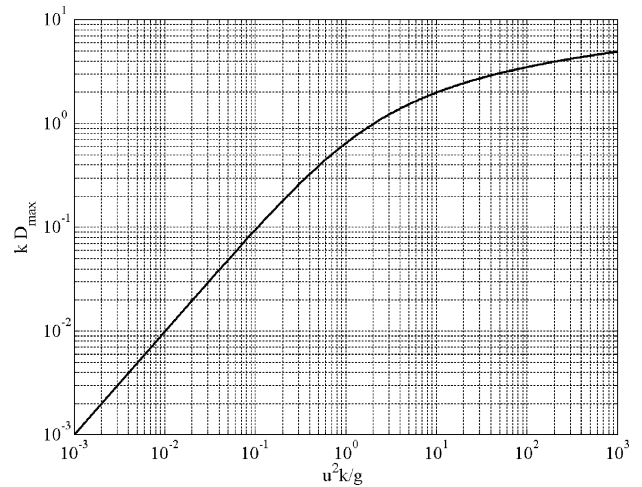


Fig. 3. Values of D_{\max} to be used in Eq. (17). D_{\max} (m); u (m/s); k (m^{-1}); g (m^2/s).

3.6. The ‘‘minimum distance’’ assumption

A further simplification of the model, that avoids the necessity of a cumbersome numerical calculation to verify the impact condition and to calculate the $\Delta\theta$ and $\Delta\varphi$ intervals is given by the ‘‘minimum distance’’ assumption. In this approach, the probability (or possibility) that the fragment passes over the target is neglected. With reference to Fig. 2(b), this is equivalent to assume that for all the values of φ higher than φ_{\min} the impact condition is verified. This condition is strictly valid only for ‘‘high’’ targets at a ‘‘sufficient’’ distance from the fragment origin. In all other cases, the assumption leads to over conservative results that may be used only as a preliminary estimate of impact probabilities. Using this simplification, the following function could be obtained to evaluate the probability of impact of the fragment on the target:

$$P_{\text{imp,F}}(k, u) \cong \frac{\Delta\theta}{2\pi} [0.5 - \text{PI}] \quad (16)$$

where no rebounding was considered for negative values of φ , and PI has the following expression:

$$\text{PI} = z_1 \times \frac{D_{\min}}{D_{\max}} + z_2 \times \left(\frac{D_{\min}}{D_{\max}} \right)^{20} + (0.5 - z_1 - z_2) \times \exp \left[z_3 \times \frac{D_{\min} - D_{\max}}{D_{\min}} \right] \quad (17)$$

where D_{\max} is the maximum distance achievable by the fragment (dependent both by k and u), D_{\min} the minimum distance of the target from the fragment source position (e.g. $D_{\min} = D - R$ in Fig. 1(b)) and the z_1 , z_2 and z_3 parameters are dependent on the drag factor k and the initial velocity u . Fig. 3 may be used to evaluate the values of D_{\max} and Fig. 4 may be used to evaluate the parameters z_1 , z_2 and z_3 to be used in Eq. (17) on the basis of the values of k and u . Thus, the ‘‘minimum distance’’ assumption allows the

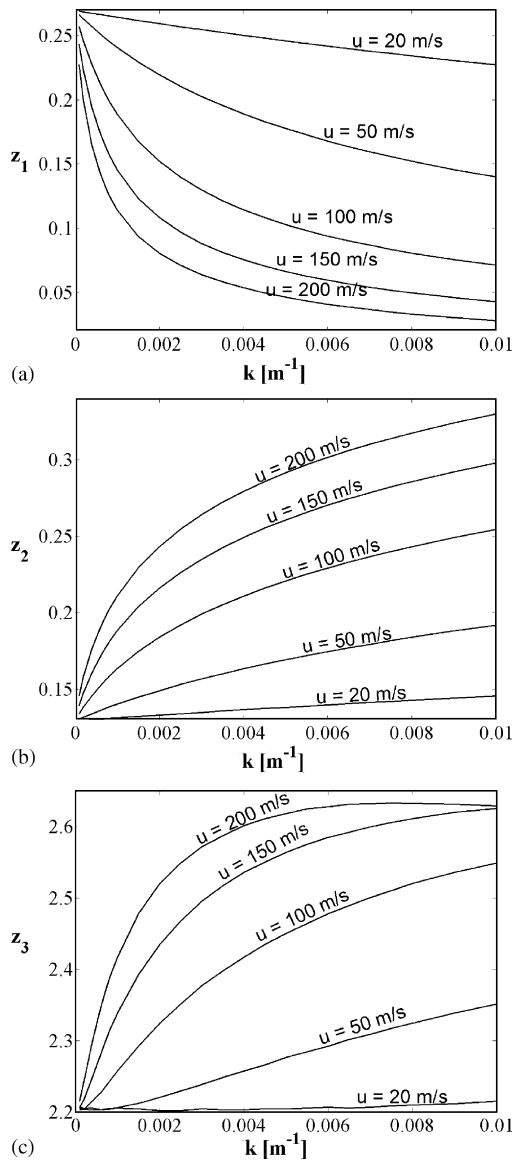


Fig. 4. Values of parameters z_1 (a), z_2 (b) and z_3 (c) to be used in Eq. (17).

direct and straightforward calculation of the fragment impact probability by the use of Figs. 3 and 4, and of Eqs. (6) and (7).

4. Results and discussion

4.1. Definition of case studies

In order to understand the results obtained with the model developed, a range of case studies was defined. Fragments having different shape, mass, and initial velocity were considered. The values of mass and initial velocities were chosen in order to well represent the reasonable range of these parameters experienced in past accidents.

Tables 2 and 3 show the fragment geometries used in the case studies. Several fragment shapes were considered: hemi-

spherical caps, cylindrical pipes, pipe curves, and more complex geometries. For each shape, several fragment sizes were considered.

The mass of the fragments used in the case studies ranged between 40 and 4000 kg. This resulted in a difference of about an order of magnitude in the drag constant k . It must be recalled that in the present approach, the drag factor k is the only parameter dependent on fragment characteristics that is used in the ballistic model.

For each fragment, four different initial velocities were considered: 50, 100, 150 and 200 m/s, respectively. The approach described in Section 3 was applied in order to calculate the impact probabilities.

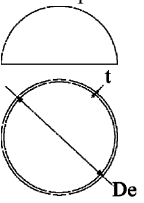
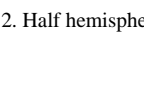
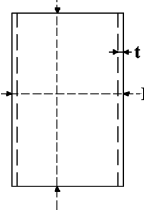
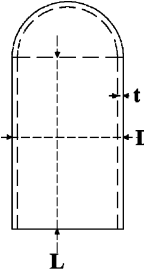
Two different types of target were considered: a column (vertical cylinder with a high height/radius (H_T/R_T) ratio) and a vertical atmospheric tank (vertical cylinder with a low H_T/R_T ratio). Several distances and sizes were used in the simulations. Table 4 summarises the different geometrical characteristics chosen for the targets. The importance and the influence of the different model parameters were evaluated on the basis of the defined case studies. The geometries considered for the fragment and for the target, as well as the wide range of initial velocities, resulted in a number of representative case studies for the analysis and the validation of model results.

4.2. Results of model application to case studies

Fig. 5 shows the calculated impact probabilities obtained for two case studies. In Fig. 5(a), the impact probabilities of fragment F1 (hemispherical end) with an initial velocity of 50 m/s were calculated as a function of target distance for all the targets described in Table 4. In Fig. 5(b), the impact probabilities were calculated for fragment F5 (tube curve) with an initial velocity of 200 m/s. Qualitatively similar results were obtained for all the other fragments and velocities, and were not reported for the sake of brevity. In all the case studies, impact probabilities always resulted below 10^{-1} for credible values of target distances and sizes, and fell below 10^{-2} for target distances higher than 50 m. Fig. 5 well evidences that the trend of the impact probability with respect to target distance is almost the same in all the considered cases, and is only slightly influenced by the target shape and by the geometrical parameters of the fragment. The impact probability decreases almost linearly on the log–log plot, with the exception of distance values very near to the maximum projection distance. In this region, the lower dependence of the projection distance on the projection angle φ results in a strong increase of the $\Delta\varphi$ value that identifies all the trajectories able to cause the impact (see Eq. (10)).

The influence of target size and shape on the values of impact probability is important. As expected, higher impact probabilities correspond to larger sizes of targets having the same shape. This is evident if the curves corresponding to targets T1–T5 and T6–T8 are compared. The target shape also influences the probability values. At sufficient distances

Table 2
Types and geometrical characteristics of the fragments used in the case studies (part 1)

| Fragment type | ID | De (m) | <i>t</i> (m) | <i>L</i> (m) | <i>M</i> (kg) | <i>k</i> (m ⁻¹) | | |
|--|-----|--------|--------------|--------------|---------------|--|-----------------------|-----------------------|
| | | | | | | Min | Max | Average |
| 1. Hemispherical  | F1 | 1.6 | 0.015 | – | 480 | 6.6×10^{-4} | 1.30×10^{-3} | 9.8×10^{-4} |
| | F2 | 1.6 | 0.025 | – | 810 | 3.7×10^{-4} | 7.7×10^{-4} | 5.7×10^{-4} |
| | F3 | 2 | 0.02 | – | 1000 | 4.8×10^{-4} | 9.8×10^{-4} | 7.3×10^{-4} |
| | F4 | 2 | 0.04 | – | 2040 | 2.2×10^{-4} | 4.7×10^{-4} | 3.4×10^{-4} |
| 2. Half hemispherical  | F7 | 1.6 | 0.015 | – | 240 | 6.6×10^{-4} | 1.30×10^{-3} | 9.8×10^{-4} |
| | F8 | 1.6 | 0.025 | – | 405 | 3.7×10^{-4} | 7.7×10^{-4} | 5.7×10^{-4} |
| | F9 | 2 | 0.02 | – | 500 | 4.8×10^{-4} | 9.8×10^{-4} | 7.3×10^{-4} |
| 3. Cylindrical shell  | F10 | 2 | 0.04 | – | 1020 | 2.2×10^{-4} | 4.7×10^{-4} | 3.4×10^{-4} |
| | F11 | 1.6 | 0.015 | 0.8 | 466 | 1.9×10^{-4} | 2.24×10^{-3} | 1.21×10^{-3} |
| | F12 | 1.6 | 0.025 | 0.8 | 771 | 1.9×10^{-4} | 1.34×10^{-3} | 7.7×10^{-4} |
| | F13 | 1.6 | 0.015 | 1.6 | 932 | 8×10^{-5} | 2.24×10^{-3} | 1.16×10^{-3} |
| | F14 | 1.6 | 0.025 | 1.6 | 1543 | 8×10^{-5} | 1.34×10^{-3} | 7.1×10^{-4} |
| | F15 | 2 | 0.02 | 2 | 1940 | 6×10^{-5} | 1.67×10^{-3} | 8.7×10^{-4} |
| 4. Cylindrical shell + Hemispherical  | F16 | 2 | 0.04 | 2 | 3840 | 6×10^{-5} | 8.3×10^{-4} | 4.4×10^{-4} |
| | F17 | 1.6 | 0.015 | 1.6 | 1412 | 4.2×10^{-4} | 7.9×10^{-4} | 6.1×10^{-4} |
| | F18 | 1.6 | 0.025 | 1.6 | 2023 | 2.9×10^{-4} | 5.4×10^{-4} | 4.1×10^{-4} |
| | F19 | 2 | 0.02 | 2 | 2420 | 3.9×10^{-4} | 7.1×10^{-4} | 5.5×10^{-4} |
| | F20 | 2 | 0.04 | 2 | 4320 | 2.0×10^{-4} | 3.8×10^{-4} | 2.9×10^{-4} |
| Average <i>k</i> interval | | | | | | $(2.9 \times 10^{-4}) / (1.21 \times 10^{-3})$ | | |

De: external diameter; *t*: thickness; *L*: length; *M*: mass; *k*: drag factor.

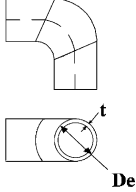
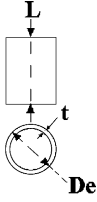
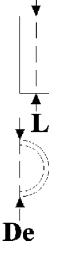
of the target (higher than 20 m) the probabilities of impact on targets having similar H_T/R_T values are very near, even if the H_T/R_T ratio of the target is not the same. The H_T/R_T ratio only plays a role at limited distances of the target (lower than 20 m), since in this region the value of target radius, R_T , is the more important parameter for the impact probability.

Fig. 6 reports the values of the impact probabilities obtained with the “minimum distance” assumption for the case studies of Fig. 5. As shown in the figure, the application of the “minimum distance” assumption leads to more conservative values of impact probability. Fig. 7 shows a comparison between the probability values obtained with the complete model and using the “minimum distance” assumption. The figure evidences that the difference between the two models may be as high as an order of magnitude, although in a region where the absolute values of probabilities are below 10^{-2} for both the models. Similar results were obtained for

all the case studies defined in the previous section. The difference between the impact probabilities always resulted below 3×10^{-2} in all the case studies. Thus, it may be concluded that the use of the “minimum distance” assumption leads to conservative results and to impact probabilities slightly higher than those obtained with the complete model. However, the much higher simplicity of impact probability estimation by the application of the “minimum distance” assumption makes useful this approach for a preliminary estimation of the upper boundary of the impact probability values.

The influence of the fragment mass and shape on the impact probability is limited. Fig. 8(a) shows the values of impact probabilities as a function of target distance for fragments F1 and F4 (spherical bottoms) projected with an initial velocity of 100 m/s on target T5. The curves obtained for all the other spherical bottoms fall within the curves for fragments F1 and F4, and were not reported. Fig. 8(b) shows the

Table 3
Types and geometrical characteristics of the fragments used in the case studies (part 2)

| Fragment type | ID | De (m) | t (m) | L (m) | M(kg) | k (m ⁻¹) | | |
|--|-----|--------|--------|-------|-------|---|-----------------------|-----------------------|
| | | | | | | Min | Max | Average |
|  1. Tube curve 3D UNI 7929 | F5 | 0.32 | 0.0071 | – | 40 | 3.25×10^{-3} | 4.9×10^{-3} | 4.10×10^{-3} |
| | F6 | 0.61 | 0.0125 | – | 266 | 1.80×10^{-3} | 2.73×10^{-3} | 2.26×10^{-3} |
|  2. Tube | F21 | 0.324 | 0.0071 | 0.362 | 20 | 4.7×10^{-4} | 4.83×10^{-3} | 2.65×10^{-3} |
| | F22 | 0.324 | 0.0071 | 0.724 | 40 | 2.2×10^{-4} | 4.83×10^{-3} | 2.52×10^{-3} |
| | F23 | 0.61 | 0.0125 | 0.727 | 130 | 2.2×10^{-4} | 2.73×10^{-3} | 1.47×10^{-3} |
| | F24 | 0.61 | 0.0125 | 1.454 | 266 | 0.9×10^{-4} | 2.73×10^{-3} | 1.41×10^{-3} |
|  3. Half tube | F25 | 0.324 | 0.0071 | 0.362 | 10 | 4.7×10^{-4} | 9.70×10^{-3} | 5.08×10^{-3} |
| | F26 | 0.324 | 0.0071 | 0.724 | 20 | 2.2×10^{-4} | 9.70×10^{-3} | 4.96×10^{-3} |
| | F27 | 0.61 | 0.0125 | 0.727 | 65 | 2.2×10^{-4} | 5.49×10^{-3} | 2.85×10^{-3} |
| | F28 | 0.61 | 0.0125 | 1.454 | 133 | 0.9×10^{-4} | 5.49×10^{-3} | 2.79×10^{-3} |
| Average k interval | | | | | | $(1.41 \times 10^{-3})/(5.08 \times 10^{-3})$ | | |

De: external diameter; t: thickness; L: length; M: mass; k: drag factor.

same results obtained for fragments F5 and F6 (tube curves). The results in Fig. 8 confirm that the differences in the impact probabilities are always very low for fragments of the same shape and hence with drag factor of the same order of magnitude. Differences in impact probabilities caused by the drag factor for fragment having the same shape resulted always lower than 3×10^{-3} in all the case studies.

However, Fig. 9 shows that also the influence of the geometrical shape of the fragment is minimum. Fig. 9(a) compares the impact probabilities as a function of target distance for fragments with mass of the same order of magnitude but

with different shape: F1 (spherical bottom), F6 (tube curve) and F24 (cylindrical pipe). In Fig. 9(b), the impact probabilities are compared for fragments having different shape and mass, but similar drag factors. The figure evidences that almost negligible differences are present, confirming that fragments having the same drag factor result in the same impact probability.

The results in Fig. 9 evidence that the influence of drag factor on the impact probability is limited over all the wide range of fragment shapes and masses explored in the present study. The maximum difference in probability values due to differences in drag factors was always lower than 4×10^{-3} for all the case studies considered, even if, as shown in Tables 2 and 3, the fragments used in the case studies have differences higher than an order of magnitude in the drag factor, that ranges from 2.9×10^{-4} to $5.08 \times 10^{-3} \text{ m}^{-1}$. The limited influence of the drag factor on the impact probabilities confirms the validity of the present approach, where only a mean value of the drag factor is introduced in the model, based on the geometry of the fragment. The above results point out that errors in the estimation of the drag factor (e.g. due to fragment orientation) are unlikely to cause relevant errors in model predictions.

Table 4
Size of the targets used in the case studies

| ID | Description | H _T (m) | R _T (m) | H _T /R _T | H _T R _T (m ²) |
|----|--|--------------------|--------------------|--------------------------------|---|
| T1 | Atmospheric vessel 25 m ³ | 4.75 | 1.35 | 3.5 | 6.4 |
| T2 | Atmospheric vessel 100 m ³ | 7.47 | 2.2 | 3.3 | 16.4 |
| T3 | Atmospheric vessel 500 m ³ | 11.6 | 3.9 | 3 | 45.2 |
| T4 | Atmospheric vessel 1000 m ³ | 6.9 | 7.5 | 0.92 | 51.7 |
| T5 | Atmospheric vessel 5200 m ³ | 12.3 | 12.5 | 0.98 | 153.7 |
| T6 | Column | 10 | 0.5 | 20 | 5 |
| T7 | Column | 20 | 1 | 20 | 20 |
| T8 | Column | 40 | 2 | 20 | 80 |

H_T: target height; R_T: target radius.

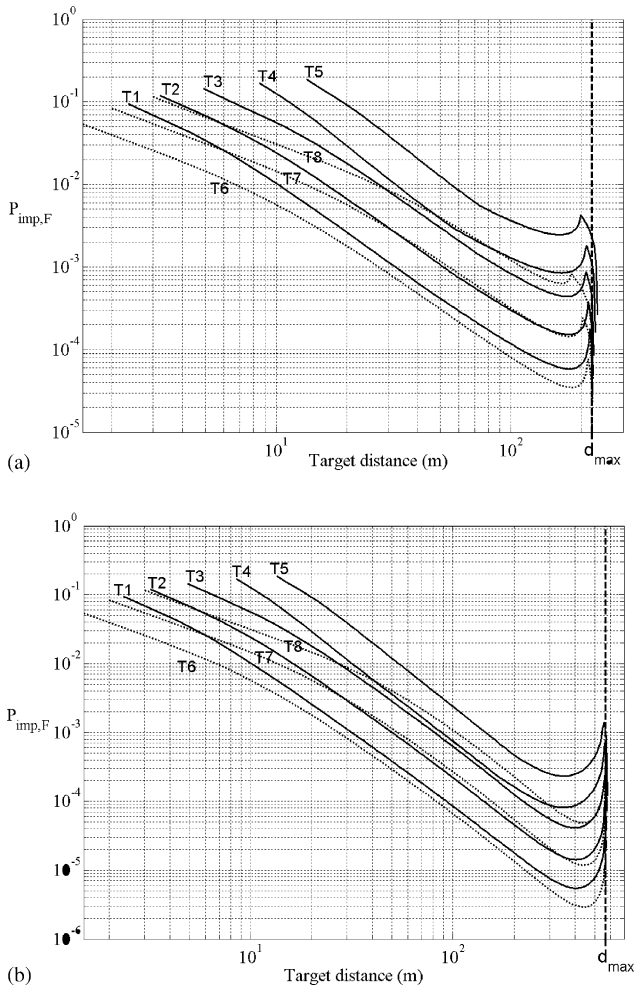


Fig. 5. Probability of impact as a function of target distance for two different case studies. (a) Fragment F1, initial velocity 50 m/s (D_{max} 221 m); (b) Fragment F5, initial velocity 200 m/s (D_{max} 567 m).

The influence of fragment initial velocity is well evidenced in Fig. 7. The figure evidences that the initial velocity mainly influences the maximum distance that may be reached by the fragment. However, the probability that a fragment will reach the higher values of distance rapidly decreases, thus leaving almost unaltered the impact probabilities at lower distances. In these zones, the maximum probability difference caused by differences in initial velocity was always lower than 3×10^{-3} in all the case studies considered. This results in curves of impact probability with respect to target distance that are almost coincident for all the range of credible subsonic values of initial velocities. The only difference is that higher initial velocities result in non-zero impact probability values at higher target distances, due to the higher maximum distances of fragment projection. Therefore, it may be concluded that the initial velocity is a critical parameter in the determination of the maximum possible projection distance of the fragment, but not in the determination of impact probabilities. As a matter of fact, the impact probabilities at distances lower than the maximum projection distance are scarcely affected by this

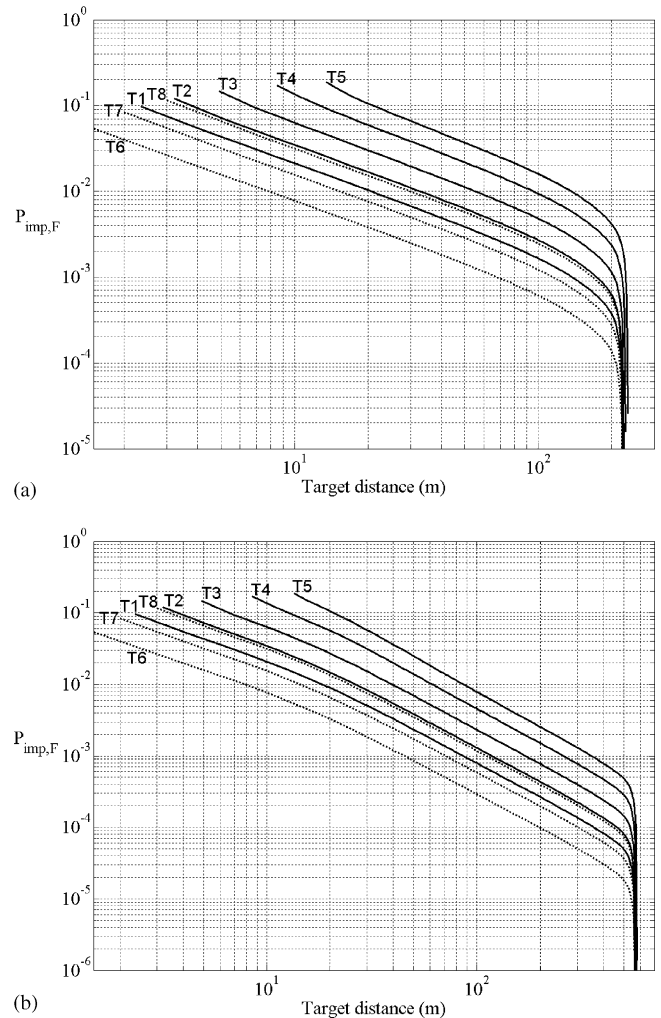


Fig. 6. Probability of impact calculated with the “minimum distance” assumption for the case studies shown in Fig. 5. (a) Fragment F1, initial velocity 50 m/s (D_{max} 221 m); (b) Fragment F5, initial velocity 200 m/s (D_{max} 567 m).

parameter. This suggests that in a conservative approach, the higher credible initial projection velocity should be assumed for the estimation of impact probability.

Figs. 5 and 7 also show the correlation between the maximum flight distance and the impact probability. These data may be used to estimate safety distances for domino effect caused by fragments that may be of interest as cut-off criteria in QRA as well as in land use planning [25].

4.3. Model validation

Holden and Reeves [11] report data on missile projection following the BLEVE of seven LPG spheres. In particular, for all the accidents analyzed, the study reports the number of fragments generated, the maximum distance of fragment projection and a curve relating the value of the distance from the explosion, R , to the fraction F of fragments projected at distances lower than R . The $F(R)$ curve, shown in Fig. 10,

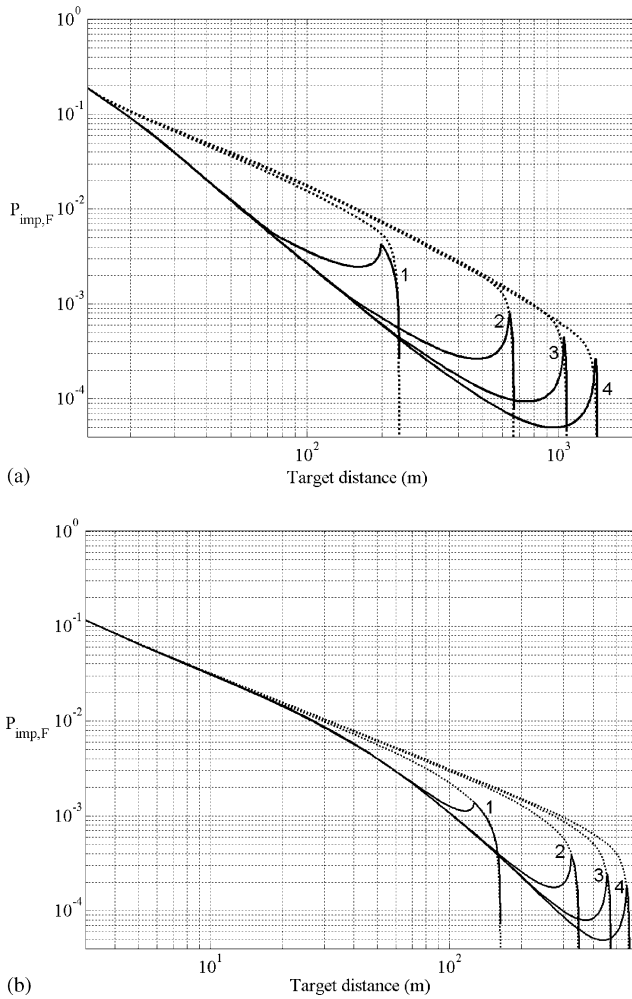


Fig. 7. Influence of initial velocity and comparison of the impact probabilities calculated with the complete model (solid lines) and using the “minimum distance” assumption (dotted lines). Initial velocities: (1) 50 m/s; (2) 100 m/s; (3) 150 m/s; (4) 200 m/s. (a) Target T5, fragment F1; (b) target T8, fragment F5.

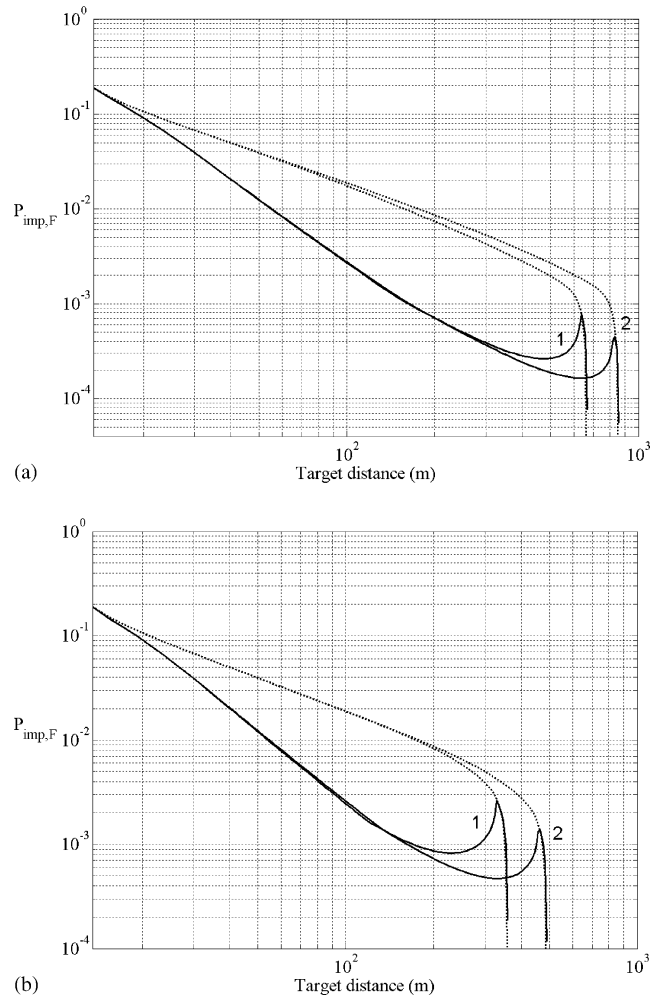


Fig. 8. Influence of drag factor on impact probability. Continuous line: complete model; dotted line: “minimum distance assumption”. Initial velocity 100 m/s, target T5. (a) 1: fragment F1 ($k = 9.80 \times 10^{-4} \text{ m}^{-1}$), 2: fragment F4 ($k = 3.4 \times 10^{-4} \text{ m}^{-1}$); (b) 1: fragment F5 ($k = 4.10 \times 10^{-3} \text{ m}^{-1}$), 2: fragment F6 ($k = 2.26 \times 10^{-3} \text{ m}^{-1}$).

was obtained from the analysis of available data for all the accidents considered.

The results of Holden and Reeves [11] were used to carry out a preliminary validation of the approach developed in the present study. The model previously described was applied to the calculation of the $F(R)$ function for the accidental events analysed by Holden and Reeves [11], and the results were compared with the data shown in Fig. 10. This was possible introducing a few assumptions:

1. a number of fragments equal to that actually formed in each accident was considered;
2. each fragment was considered to have a spherical cap shape, with a mass equal to that estimated for the entire vessel and divided by the number of fragments generated.

The latter hypothesis is commonly adopted when fragments mass distributions are not available [10,14,16]. These

assumptions allowed the calculation of the drag factors by the above-described procedure, on the basis of the mass of the vessel that undergoes the fragmentation.

The maximum initial projection velocity ($u_{\max,F}$) of the fragments was estimated from the data on the maximum distance reached by the fragments in each accident. A minimum initial projection velocity ($u_{\min,F}$) of 20 m/s was assumed. A uniform probability was assumed for the initial velocity of each fragment between the minimum and maximum values estimated. Data used for model validation are summarized in Table 5.

Fig. 10 reports the results of the above calculations. These clearly point out that the model developed, with the introduction of few simplifying assumptions, well predicts the distribution of fragment projection distances experienced in a number of accidental events. This was confirmed by the results of a χ^2 -test performed on the results of the present study. A p -value of 60% was obtained, thus confirming the sufficient

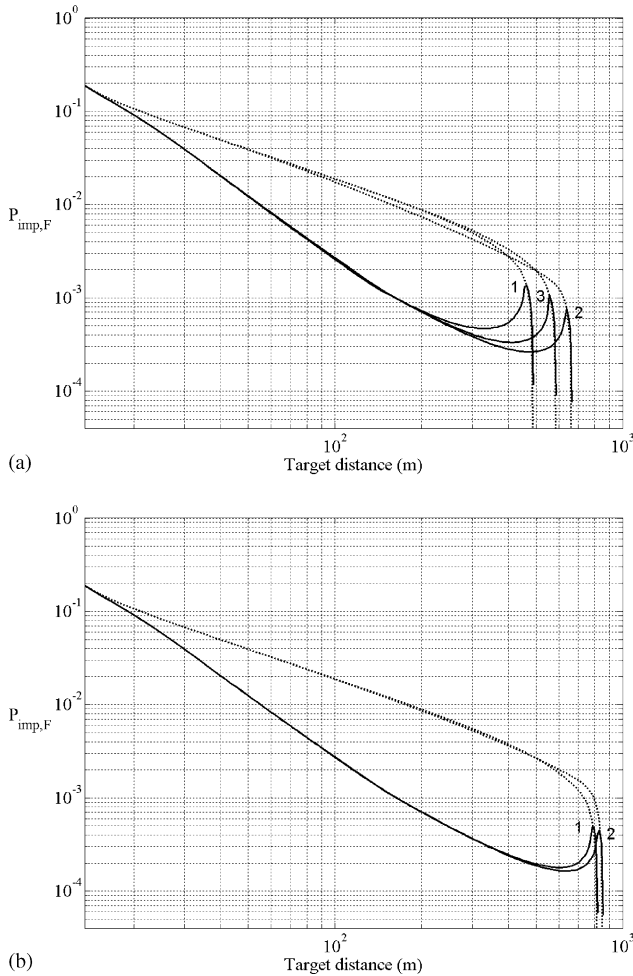


Fig. 9. Influence of drag factor on impact probability. Continuous line: complete model, dotted line: “minimum distance assumption”. Initial velocity of fragments: 100 m/s, target T5. (a) 1: fragment F6 ($k = 2.26 \times 10^{-3} \text{ m}^{-1}$), 2: fragment F1 ($k = 9.8 \times 10^{-4} \text{ m}^{-1}$), 3: fragment F24 ($k = 1.41 \times 10^{-3} \text{ m}^{-1}$); (b) 1: fragment F16 ($k = 4.4 \times 10^{-4} \text{ m}^{-1}$), 2: fragment F4 ($k = 3.4 \times 10^{-4} \text{ m}^{-1}$).

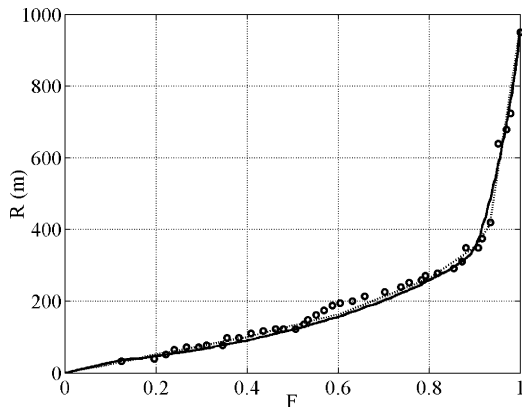


Fig. 10. Fraction of the total fragments, F , projected at a distance lower than R . Dots: data from the analysis of past accidents [11]. Dotted line: best fit of data from past accidents [11]. Continuous line: model developed in the present study.

Table 5

Data used in the model validation with Holden and Reeves [11] data on LPG spherical vessel BLEVEs

| $V \text{ (m}^3\text{)}$ | $t \text{ (mm)}$ | N_F | $D_{\text{max}} \text{ (m)}$ | $k \text{ (m}^{-1}\text{)}$ | $u_{\text{max}} \text{ (m/s)}$ |
|--------------------------|------------------|-------|------------------------------|-----------------------------|--------------------------------|
| 800 | 27 | 4 | 320 | 10^{-3} | 62 |
| 800 | 27 | 5 | 320 | 10^{-3} | 62 |
| 800 | 27 | 5 | 320 | 10^{-3} | 62 |
| 1200 | 31 | 3 | 325 | 8.7×10^{-4} | 62 |
| 1200 | 31 | 5 | 325 | 8.7×10^{-4} | 62 |
| 1600 | 34 | 16 | 950 | 7.3×10^{-4} | 123 |
| 2300 | 39 | 19 | 350 | 6.4×10^{-4} | 63 |

V : volume of spherical vessel; N_F : number of fragment generated in each explosion; D_{max} : maximum distance reached by the fragments; k : evaluated drag factor; u_{max} : assumed maximum initial velocity.

quality of the fit of the model developed in the present study to the data of Holden and Reeves [11].

5. Conclusions

A model was developed for the assessment of the impact probability on a given target of fragments generated in the internal explosion of a process vessel. The model was based on the analytical solution of the ballistic equations for fragment trajectory, and on the introduction of probability distribution functions for the initial direction of projection of the fragment. A preliminary validation based on literature data showed that this approach is able to correctly represent the distribution of projection distances experienced in accidental events.

The model needs three uncertain input parameters: the mass, the shape and the initial velocity of the fragment. However, the parametric analysis of model results evidenced that the mass and shape of the fragment, that are comprised in the fragment drag factor, are not likely to have a relevant influence on the impact probability. Also, the initial velocity was shown to play a limited role on the values of impact probability at a given distance, although the maximum projection distance is highly dependent on this parameter. However, the results obtained showed that conservative values of impact probability are obtained considering the highest credible initial velocities for the fragment on the basis of the explosion strength.

Impact probabilities calculated for a number of representative case studies always resulted below 10^{-1} , and were always lower than 10^{-2} for secondary targets at distances higher than 50 m. The “minimum distance” assumption, that makes possible to neglect the actual target shape function in the calculation of impact condition, leads to conservative results, with a maximum error in probability values of 3×10^{-2} . However, it was shown that this assumption allows a relevant reduction of the calculation effort needed for model application, and may thus be used for a preliminary assessment of impact probabilities.

Therefore, it may be concluded that the approach developed is suitable for the estimation of the fragment im-

probabilities in a QRA framework, allowing both a preliminary identification of possible “domino events” caused by fragments and a detailed calculation of impact probability, taking into account the geometrical constraints of the problem.

Acknowledgments

Financial support from CNR – Gruppo Nazionale per la Difesa dai Rischi Chimico-Industriali ed Ecologici is gratefully acknowledged.

Appendix A

In the following the solution of Eqs. (11) and (12) is given for positive values of angle φ (see Fig. 2).

• Solution of Eq. (1)

$$\dot{x}(t) = \frac{u \cos(\varphi)}{1 + k \times t \times u \cos(\varphi)} \quad (\text{A.1})$$

$$x(t) = \frac{1}{k} \ln(1 + k \times t \times u \cos(\varphi)) \quad (\text{A.2})$$

• Solution of Eq. (2)

Ascending part:

$$\dot{y}(t) = \frac{\tan([\beta - \alpha \times g \times t])}{\alpha} \quad (\text{A.3})$$

$$y(t) = -\frac{1}{2k} \ln \left[\frac{\alpha^2 \times \dot{y}(t)^2 + 1}{\alpha^2 \times (u \sin(\varphi))^2 + 1} \right] \quad (\text{A.4})$$

Descending part:

$$\dot{y}(t) = \frac{1 - \exp(\chi t - 2\beta)}{\alpha \times [1 + \exp(\chi t - 2\beta)]} \quad (\text{A.5})$$

$$y(t) = Y_M + (2k)^{-1} \ln[1 - \alpha^2 \times \dot{y}(t)^2] \quad (\text{A.6})$$

where $\alpha = (k/g)^{0.5}$; $\beta = a \tan(\alpha \times u \sin(\varphi))$; $\chi = 2k/\alpha$; $Y_M = (2k)^{-1} \ln[\alpha^2 \times (u \sin(\varphi))^2 + 1]$

References

- [1] F.P. Lees, Loss Prevention in the Process Industries, second ed., Butterworth-Heinemann, Oxford, UK, 1996.
- [2] CCPS, Guidelines for Chemical Process Quantitative Risk Analysis, second ed., AIChE, New York, 2000.
- [3] G.N. Pettitt, R.R. Schumacher, L.A. Seeley, Evaluating the probability of major hazardous incidents as a result of escalation event, J. Loss Prev. Process Ind. 6 (1993) 37.
- [4] D.F. Bagster, R.M. Pitblado, The estimation of domino incident frequencies—an approach, Process Saf. Environ. Prot. 69 (1991) 196.
- [5] F.I. Khan, S.A. Abbasi, Models for domino effect analysis in chemical process industries, Process Saf. Prog. 17 (1998) 107.
- [6] J. Gledhill, I. Lines, Development of methods to assess the significance of domino effects from major hazard sites, CR Report 183, Health and Safety Executive (1998).
- [7] V. Cozzani, S. Zanelli, An approach to the assessment of domino accidents hazard in quantitative area risk analysis, in: Proceedings of the 10th International Symposium on Loss Prevention and Safety Promotion in the Process Industries, Elsevier, Amsterdam, 2001, pp. 1263–1274.
- [8] V. Cozzani, E. Salzano, The quantitative assessment of domino effect caused by overpressure. Part I: probit models, J. Hazard. Mater. 107 (2004) 67.
- [9] V. Cozzani, E. Salzano, The quantitative assessment of domino effect caused by overpressure. Part II: case studies, J. Hazard. Mater. 107 (2004) 81.
- [10] CCPS, Guidelines for Evaluating the Characteristics of Vapor Cloud Explosions, Flash Fires and BLEVEs, AIChE, New York, 1994.
- [11] P.L. Holden, A.B. Reeves, Fragment hazards from failures of pressurised liquefied gas vessels, in: IChemE Symposium Series No. 93, 1985, p. 205.
- [12] N.F. Scilly, J.H. Crowter, Methodology for predicting domino effects from pressure vessel, in: International Conference on Hazard Identification and Risk Analysis, Human Factors and Human reliability in Process Safety, 1992, p. 1.
- [13] W.E. Baker, P.A. Cox, P.S. Westine, J.J. Kulesz, R.A. Strehlow, Explosion Hazards and Evaluation, Elsevier, Amsterdam, 1983.
- [14] U. Hauptmanns, A Monte Carlo-based procedure for treating the flight of missiles from tank explosions, Probab. Eng. Mech. 16 (2001) 307–312.
- [15] U. Hauptmanns, A procedure for analyzing the flight of missiles from explosions of cylindrical vessels, J. Loss Prev. Process Ind. 14 (2001) 395–402.
- [16] H.L. Brode, Blast wave from a spherical charge, Phys. Fluids. 2 (1959) 217.
- [17] M.R. Baum, The velocity of missiles generated by the disintegration of gas pressurised vessel and pipes, 106, 1984, 362–368.
- [18] B.E. Gelfand, S.M. Frolov, A.M. Bartenev, Calculation of the rupture of a high pressure reactor vessel, Combustion Explosion and Shock Waves 24-4 (1989) 488–496.
- [19] M.R. Baum, Disruptive failure of pressure vessels: preliminary design guidelines for fragment velocity and the extent of the hazard zone, in: Advances in Impact Blast Ballistics and Dynamic Analysis of Structures, ASME PVP, New York, 1987.
- [20] C.V. Moore, the design of barricades for hazardous pressure systems, Nucl. Eng. Des. 5 (1967) 81–97.
- [21] C.J.H. Van Den Bosh, R.A.P.M. Weterings, Methods for the calculation of physical effects (Yellow Book), third ed., Committee for the Prevention of Disasters, The Hague, NL, 1997.
- [22] M.R. Baum, Rupture of a gas pressurised cylindrical vessel: the velocity of a detached end-cap, J. Loss Prev. Process Ind. 8 (3) (1995) 149–161.
- [23] M.R. Baum, Failure of a horizontal pressure vessel containing a high temperature liquid: the velocity of end-cap and rocket missiles, J. Loss Prev. Process Ind. 12 (1999) 137–145.
- [24] M.R. Baum, The velocity of large missiles resulting from axial rupture of gas pressurised cylindrical vessels, J. Loss Prev. Process Ind. 14 (2001) 199–203.
- [25] V. Cozzani, G. Gubinelli, G. Russo, E. Salzano, S. Zanelli, An assessment of the escalation potential in domino scenarios, in: Proceedings of the 11th International Symposium on Loss Prevention and Safety Promotion in the Process Industries, 2004, pp. 1153–1162.